Office of Energy Efficiency & Renewable Energy

National Renewable Energy Laboratory

Innovation for Our Energy Future

Liquid-Phase Deposition of CIS Thin Layers

Final Report
February 2003 — July 2005

F. Ernst and P. Pirouz
Case Western Reserve University
Cleveland, Ohio

Subcontract Report
NREL/SR-520-39341
February 2006

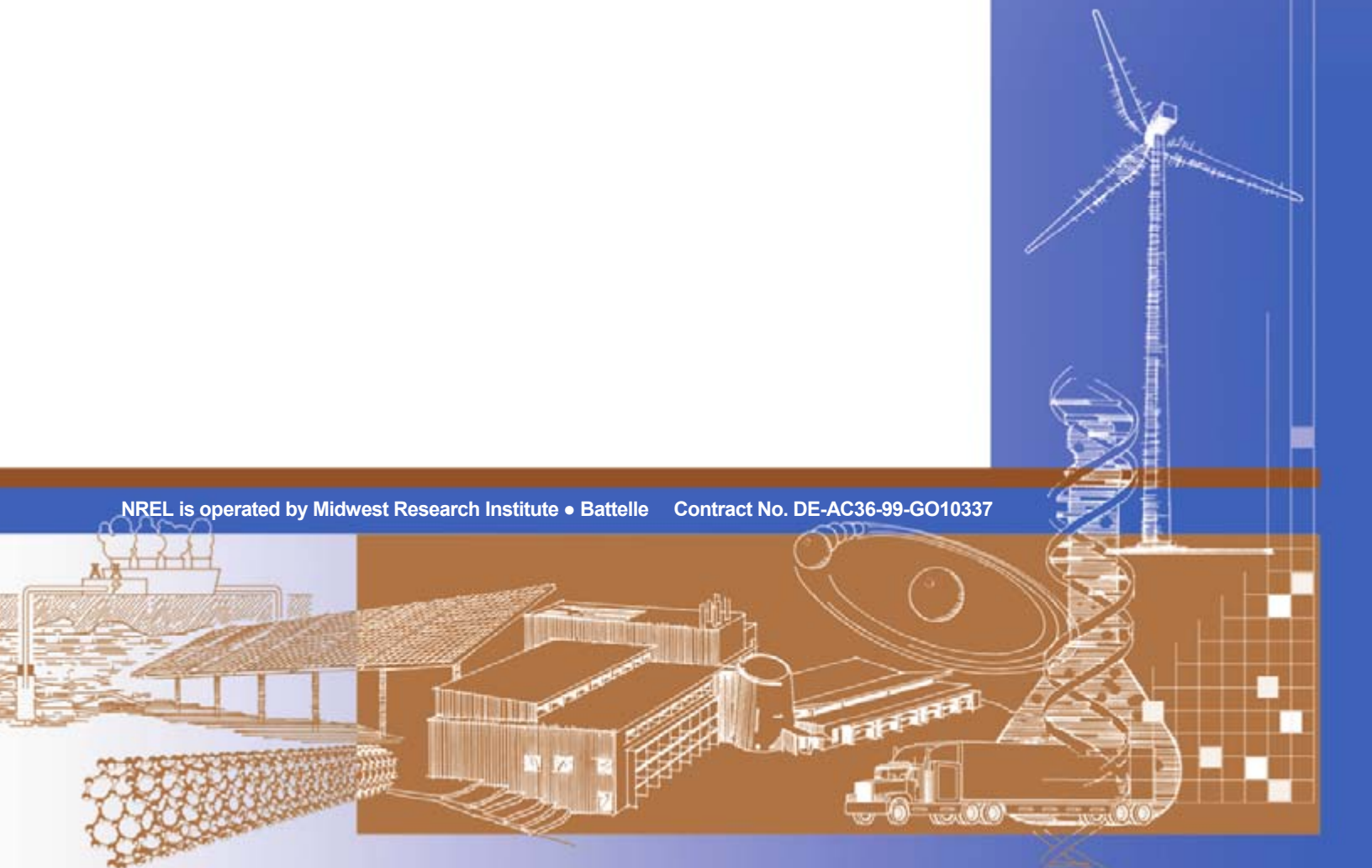

NREL is operated by Midwest Research Institute • Battelle Contract No. DE-AC36-99-GO10337

Liquid-Phase Deposition of CIS Thin Layers

Subcontract Report
NREL/SR-520-39341
February 2006

Final Report
February 2003 — July 2005

F. Ernst and P. Pirouz
Case Western Reserve University
Cleveland, Ohio

NREL Technical Monitor: B. von Roedern

Prepared under Subcontract No. XDJ-3-30630-33

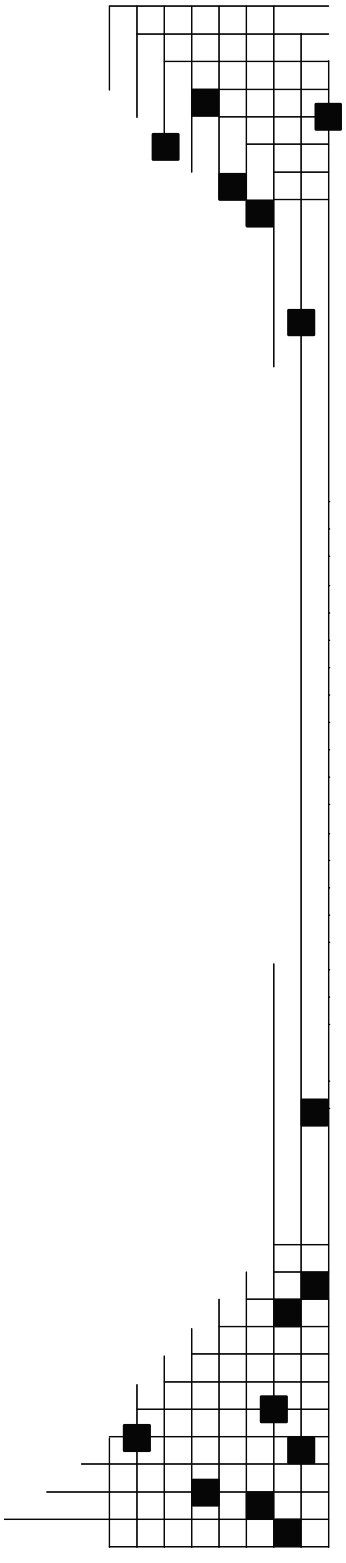

National Renewable Energy Laboratory
1617 Cole Boulevard, Golden, Colorado 80401-3393
303-275-3000 • www.nrel.gov

Operated for the U.S. Department of Energy
Office of Energy Efficiency and Renewable Energy
by Midwest Research Institute • Battelle

Contract No. DE-AC36-99-GO10337

Table of Contents

List of Figures

List of Tables

1 Liquid-Phase Deposition of α-$CuInSe_2$

The goal of the project on which this report is based was to fabricate single-phase CIS (α-Cu–In–Se, stoichiometric composition: $CuInSe_2$) thin films for photovoltaic applications from a *liquid* phase – a Cu–In–Se melt of appropriate composition. This approach of "liquid-phase deposition" (LPD) is based on the new phase diagram we have established for Cu–In–Se, the first complete equilibrium phase diagram of this system.[1–3] Fig. 1 shows the liquidus projection of the phase diagram – the surface indicating the temperature at which first solid material begins to form when cooling down from high temperatures at which the material is entirely liquid. The liquidus projection exhibits four composition fields in which the primary solid phase, i. e. the first solid material that forms on cooling down from an entirely liquid state, is α-$CuInSe_2$. Remarkably, none of the four composition fields is anywhere near the stoichiometric composition ($CuInSe_2$) of α-$CuInSe_2$.

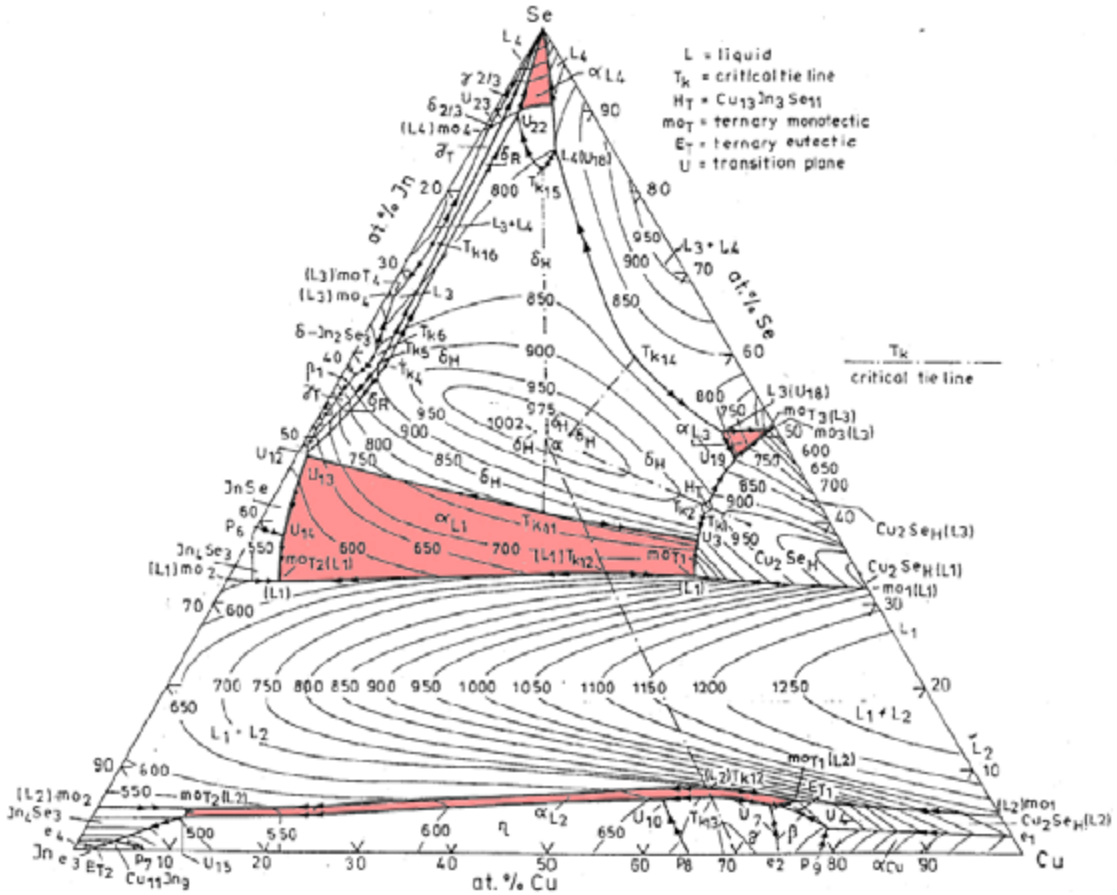

Figure 1: Liquidus projection of the Cu–In–Se phase diagram.

On freezing a melt in contact with a substrate, the solid will nucleate on the substrate. Therefore, it should be possible to grow single-phase α-$CuInSe_2$ thin-films by (i) casting a melt with a composition within one of the four relevant fields of Fig. 1 onto a substrate,

(ii) cooling it slowly to a temperature somewhat below the respective liquidus temperature, (iii) let a thin film form solidify on the substrate, and (iv) remove the remaining melt when the film has reached the desired thickness (Fig. 2).[4] The amount of melt needs to be chosen sufficiently large, such that the formation of the α-$CuInSe_2$ film, which incongruently depletes the melt of Cu, In, and Se, does not significantly alter the melt composition. Subsequently, the system is cooled to room temperature.

Since the material freezing out from the melt would be single-phase α-$CuInSe_2$ and solidifies under near-equilibrium conditions (small supercooling, small driving force), we anticipated substantially lower concentrations of structural defects than in PVD layers. This includes all varieties of structural defects: point defects, dislocations, grain boundaries, and phase boundaries (defects – by definition – are *non*-equilibrium features). Indeed, the TEM image of Fig. 3, obtained from α-$CuInSe_2$ produced during the experiments carried out to determine the new phase diagram, reveals coarse-grained, pure α-$CuInSe_2$ with a very low concentration of extended structural defects.[4]

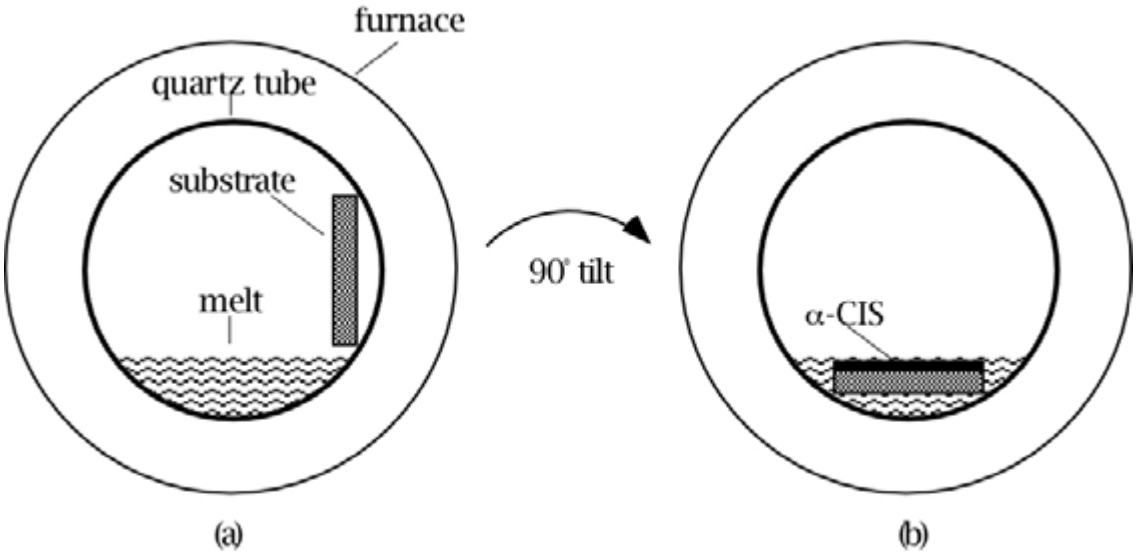

Figure 2: The concept of liquid-phase deposition (LPD). (a) $CuInSe_2$ melt with a composition in one of the shaded fields in Fig. 1. (b) Deposition of a thin α-$CuInSe_2$ film induced by slightly supercooling the melt in contact with a substrate.\

Based on the expected structural quality of the material, we anticipated substantial improvements in photovoltaic conversion efficiency. Moreover, the comparison between the anticipated, coarse-grained LPD material and fine-grained PVD material was supposed to provide deeper insight into the effect of grain boundaries on photovoltaic conversion in α-$CuInSe_2$, for which a new model was recently proposed.[5]

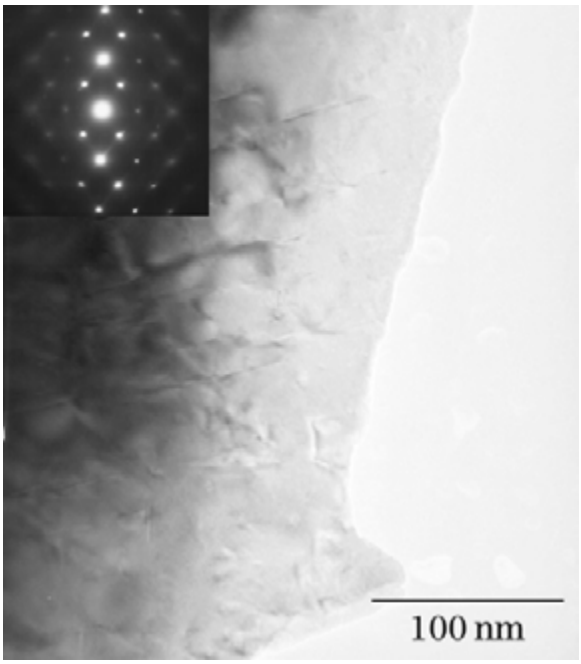

Figure 3: TEM image of α-CuInSe2 produced during experiments we carried out to determine the new phase diagram. The diffraction pattern (inset) confirms that the region imaged here is a large grain of single-phase α-CuInSe2.

2 Personnel

For the experimental part of the project, we engaged a highly qualified graduate student, Mr. Jonathan Cowen, to work on this project as part of his Ph. D. thesis. Mr. Cowen had previously received a bachelor's degree in chemistry from Cleveland State University.

3 Experimental

3.1 Encapsulation of the Elemental Starting Materials in Fused Silica Tubes

We installed a hydrogen gas tank and a gas torch sufficiently powerful for melting thick-walled fused-silica tubes with a hydrogen flame. After cutting a section with a length of about 5 cm from a fused silica tube and cleaning the inner wall surface by chemical solvents, we closed one end of the tube by melting it in the flame and then filled the tube with appropriate amounts of high-purity Cu, In, and Se. Subsequently, we evacuated the tube to a powerful rotary pump and flushed it with high-purity argon under reduced pressure (800 mbar). The latter is known to reduce the vapor pressure of Se. Finally, we sealed the ingot in the tube by closing the end connected to the pump.

3.2 Fusing of Starting Material for Liquid-Phase Deposition

Two methods were established for fusing the elemental ingots with sufficient control of the strongly exothermic fusing reaction. In the first method, we use inductive heating

provided by a high-frequency generator. The second method is to provide the required heat directly with the gas torch. Compared to fusion in a tube or muffle furnace, these methods have the advantage that we can observe the reaction through the tube walls and quickly reduce the heat supply when the reaction tends to get out of control. In the beginning, we had the problem that the fused-material showed a very strong tendency to stick to the inner wall of the fused-silica tube. It seems that this problem can be overcome by using copper with a particularly low oxygen content and thorough cleaning of the inner wall tube prior to encapsulation. Nevertheless, several iterations of fusing and knocking off sticking parts of material from the inner walls of the fused-silica tube are typically necessary before a shiny and integral piece of material is obtained that can serve for the liquid-phase deposition experiments.

3.3 Liquid-Phase Deposition in a Fused-Silica Tube

Initially, we pursued the simple method of encapsulating the ingot and the substrate in a fused-silica tube and tilting the melt over the substrate, as illustrated in 2. For fixing the substrate in the fused-silica tube, we established the following simple method: By heating the tube in the hydrogen flame from the outside, we attached a rectangular piece of fused-silica to the inner wall of the tube, such that the substrate plane was oriented normal to the wall. This setup enabled us to tilt the $CuInSe_2$ melt over the substrate simply by rotating the fused-silica tube. A problem with this preliminary method was that it can only be applied if the mismatch between the thermal expansion coefficients of the substrate material and fused silica is sufficiently small to keep the thermal stresses at the interface below a tolerable level.

3.4 Furnace

Sufficient laboratory space for the experiments was made available in the Department of Materials Science and Engineering at CWRU, as well as a furnace suitable for constructing the LPD reactor. The furnace was a three-zone horizontal tube furnace with a particularly large inner diameter hinges providing the capability of easily assessing the interior. The furnace contained a fused-silica tube with a diameter of 10 cm to give us sufficient flexibility for variations of the liquid-phase deposition experiments. The controller we used enabled us to adjust the temperature with a precision better than 1 K. Based on this furnace, we designed, constructed, and installed a reactor suitable for LPD of α-$CuInSe_2$ thin films.

3.5 The Sliding Boat Reactor

Initially, we performed experiments to deposit material by to the method illustrated in 2. For this purpose, we encapsulated the ingot material in a fused-silica ampule together with a suitable planear substrate, which was fixed to the wall of the ampoule.

Since this simple approach did not yield satisfactory results, we decided to build an entirely new, “sliding boat” reactor. In this reactor, the molten material resides in a graphite well, which is slid over the *bottom* side of several stationary substrates (“sliding

boat"). Similar sliding boat mechanisms have been utilized with great success in liquid-phase epitaxy of III–IV and IV–IV semiconductors. In order to avoid oxidation of the components or loss of selenium, we also had to construct a suitable air-tight chamber in which the sliding boat reactor could operate. Since the sliding boat reactor and the deposition chamber play a central role for the experimental results, the construction of these components is further described in the next two subsections.

3.5.1 The Deposition Chamber

The air-tight deposition chamber is shown in Fig. 4. Compared to our initial approach of encapsulating the ingot material in a fused-silica ampoule, together with a suitable substrate, the newly constructed deposition chamber substantially simplified the loading of ingot and substrates. We fitted the chamber with valves to allow pumping under vacuum as well as purging with high-purity argon gas. Depositions were carried out at pressures slightly higher than atmospheric pressure. Prior to deposition, however, the system was evacuated and heated to remove water and contaminants. Additionally, the newly constructed chamber allowed utilizing reacting gases to properly remove oxide contaminants from the surface of the substrates prior to the actual deposition. Hydrogen is often used to remove surface oxides by converting the oxides to water. The removal of surface contaminants, mainly oxides, activates the substrate surface and promotes wetting by the molten ingot. The far left of Fig. 4 shows a linear manipulator vacuum feed-through, purchased from MDC Vacuum Products Cooperation. This manipulator provided a convenient way to move the reservoir over the underlying substrates.

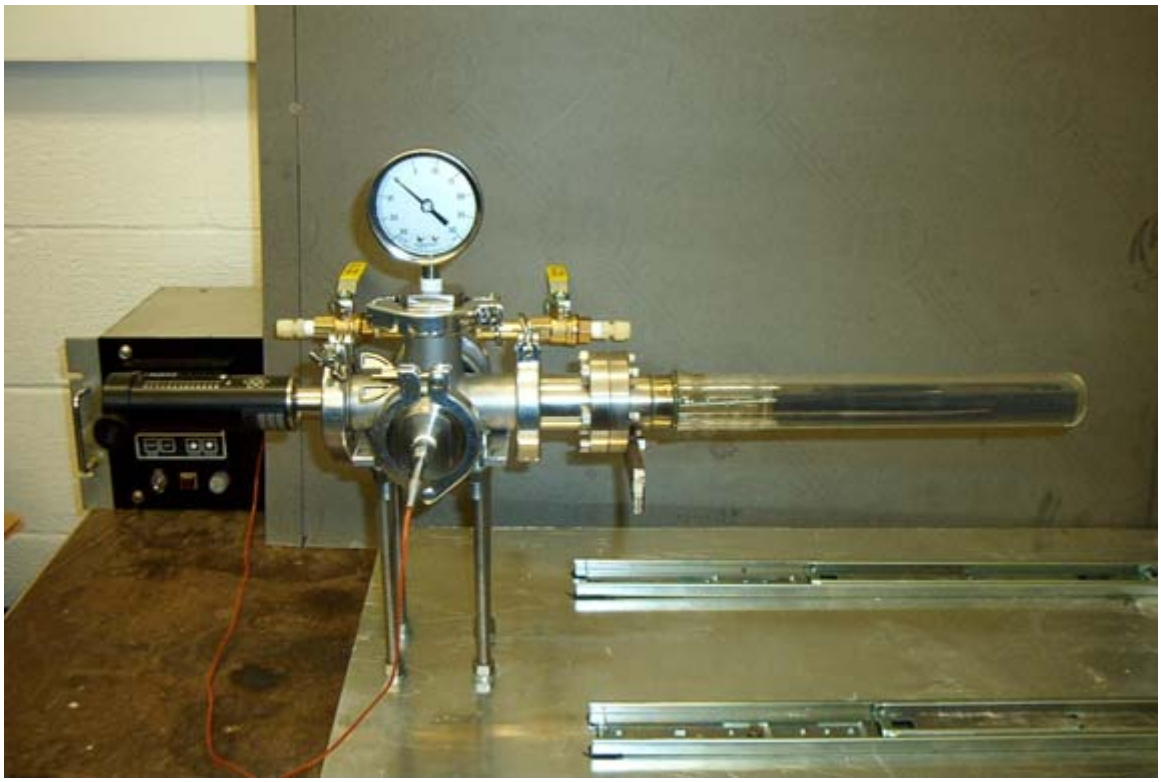

Figure 4: Deposition chamber of the new sliding-boat reactor

For the event of overheating, which could potentially result in rupture of the furnace and leakage of selenium vapor, the LPD chamber was equipped with a pressure release valve. The gas removed from the pressure release valve would run through a cold trap to condense potentially dangerous selenium vapor.

3.5.2 Sliding Boat

The sliding boat consisted of three main parts: a track, a substrate holder, and a reservoir, as shown together in Fig. 5. The outer portion or track of the boat simply provided a channel for the reservoir to slide forth and back. The substrate holder fitted nicely in the bottom of the track and below the reservoir. The construction material for the sliding was graphite. Graphite was chosen because it is available in high purity form, it is easily machined, and, mostly, because metals do not wet it.

Figure 5: Sliding boat of the new sliding-boat reactor.

3.6 Transmission Electron Microscopy

Since the primary tool for characterizing the phase composition, structure, and defects in the material we intended to fabricate was TEM (transmission electron microscopy), we have trained the graduate student in conventional, high-resolution, and analytical TEM, including electron diffraction (for phase identification). Information about the instruments we employed for this work is available on the internet.[6]

We have also trained the student in the techniques of TEM specimen preparation. This involved ion-beam milling with Ar^+ ions as the final step. In first experiments with this method, segregation of In on the specimen surface were identified as a major obstacle for obtaining high-quality TEM specimens. However, this is a known problem, and shortly after we improved the specimen quality by fine-tuning the specimen preparation parameters based on information from the literature and photovoltaic partners. Exciting new opportunities for preparing high-quality cross-sectional TEM specimens were expected from a FIB (focused ion beam system) that was delivered to the Center for Surface Analysis of Materials (administered by the Department of Materials Science and Engineering) in May 2004. However, unforeseen technical problems delayed the installation of this instrument by more than one year. Still, the instrument is not fully functional, and TEM specimens of the kind we needed for the project reviewed here cannot be obtained.

In order to obtain some first TEM specimens anyway, we continued to deposit films via our initial method of tilting the melt over the substrate, but with layers of exceedingly large thickness, generated on *purpose*. The residual stresses typically present in thick layers promotes the subsequent removal layer from the substrate, which significantly facilitates the preparation of TEM specimens compared to the case of a thick Cu-In–Se layer adherent to a substrate of a different material.

4 Results

4.1 Ingots for Liquid-Phase Deposition

Ingots for LPD were prepared from all four relevant composition fields in Fig. 1. Their compositions are listed in Table 1. The second column indicates the nominal composition (as weighed), the third column the composition after fusion, as measured by XEDS (X-ray energy-dispersive spectrometry) in a scanning electron microscope, and the fourth column the composition in the resulting LPD-thin film, again as measured by XEDS in a scanning electron microscope.

Table 1: Ingots of the $CuInSe_2$ alloys prepared and studied in Phase I

Ingot	Weighed (at %)	XEDS Ingot (at %)	XEDS Film (at %)
I1a	Cu: 12.0 In: 47.5 Se: 40.5	Cu: 8.7 In: 41.4 Se: 49.9	Cu: 4.19 In: 52.69 Se: 43.12
I1b	Cu: 32.5 In: 32.5 Se: 35.0		Cu: 24.76 In: 27.10 Se: 48.14
I1c	Cu: 46.0		Cu: 59.50

	In: 18.0 Se: 36.0		In: 15.58 Se:24.92
I2	Cu: 55.0 In: 38.5 Se: 6.5		Cu: 16.46 In: 41.47 Se: 42.08
I3	Cu 46.0 In: 4.0 Se: 50.0	Cu: 45.40 In: 2.66 Se: 51.94	Cu: 7.90 In: 1.33 Se: 90.77
I4	Cu: 2.85 In: 3.55 Se: 93.6	Cu: 4.46 In: 2.81 Se: 92.73	Cu: 5.74 In: 0.80 Se: 93.46

We have recorded XRD (X-ray diffraction) patterns, and have verified compositions by XEDS for all ingots we prepared. The results confirmed the predictions of the liquidus projection (Fig. 1). For example, one of the ingots had a Cu:In:Se ratio close to 1:1:1, but yielded layers with a Cu:In:Se ratio close to the 1:1:2 stoichiometry α-$CuInSe_2$. This confirms the basic hypothesis of our project, namely that α-$CuInSe_2$ can be (and has to be) precipitated from melts with compositions significantly *different* from 1:1:2. Not only does the stoichiometry of the deposited films correspond to the desired composition of α-$CuInSe_2$ – XRD patterns have also revealed the presence of chalcolpyrite structure of α-$CuInSe_2$.

4.2 Wetting Behavior

Initially, attempts were made to deposit α-$CuInSe_2$ thin films onto fused silica and silicon substrates. However, it soon became apparent that the surface energies of these substrates were too low to promote their sufficient wetting by the molten ingot. Silicon can be used, but requires chemical or ion etching prior to the deposition of α-$CuInSe_2$ to "activate" the surface for wetting and subsequent layer growth to occur. To overcome this wetting issue we loaded fused-silica substrates, etched with HF (hydrofluoric acid) and rinsed with dionized water, into a sputtering chamber and sputter-deposited a 1 μm thick layer of Mo, followed by a layer of 100 nm of Cu. The sputtering chamber we utilized contained three separate cathodes, thereby allowing us to deposit the Cu film right after the Mo deposition, without breaking vacuum in the chamber. The Cu layer served to passivate the Mo layer, i. e. prevented the formation of an oxide layer on the Mo. During liquid-phase deposition onto such substrates, the Cu layer diffuses into the ingot material, exposing a Mo surface with a surface energy high enough to promote uniform coverage of the substrate by the molten ingot material.
With the incorporation of these Cu-coated substrates, we were able to deposit films from all four composition fields suitable for primary precipitation of α-$CuInSe_2$, as indicated in Fig. 1.

4.3 Viscosity

In order to precipitate a thin layer of α-$CuInSe_2$ onto a substrate, the molten ingot with appropriate composition needs to be slowly cooled down to or just below the liquidus temperature indicatd by the ternary phase diagram. As expected from the usual exponential increase of the viscosity with decreasing temperature, we found that the viscosity of all ingots we tried so far rapidly increases as they are cooled down to their respective liquidus temperature. After deposition of a thin layer on the substrate, therefore, it turned out to be difficult to tilt the remaining melt off the surface of the deposited layer. Even when the substrates were turned upside down, the molten ingot did not easily release from the substrate. For this reason, the layers we have successfully deposited so far are quite thick: 10 to 15 μm. Owing to the brittleness of the deposited material and the presence of thermal stresses, a less important, but still disturbing consequence of the inappropriate layer thickness is that it is very difficult to prepare them for transmission electron microscopy, the most powerful tool for analyzing the results of our liquid-phase deposition experiments.
To circumvent these problems, we decided to deviate from the original plan and construct a laboratory-scale "sliding-boat" reactor (Section 3.5) for depositing thinner films with better surface morphology.

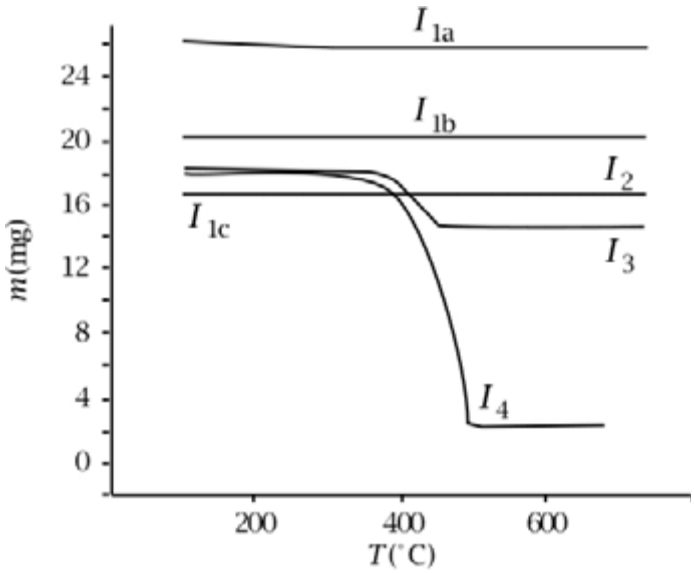

Figure 6: TGA plot of all the ingots made with compositions designated in Table 1.

4.4 Thermogravimetric Analysis

Several methods currently used for the deposition of α-$CuInSe_2$ and $CuInS_2$ require post-deposition annealing treatments in Se- or S-rich atmospheres to yield the desired chalcopyrite phase with the 1:1:2 stoichiometry. However, even when the deposited material has the correct stoichiometry, a chalcogenide-rich atmosphere is usually employed to maintain this composition. For the final construction of the sliding boat LPD reactor we had to determine at what pressures we need to operate in order to maintain the composition of the starting ingot as well as the composition of the deposited film.

Therefore TGA (thermogravimetric analysis) was employed to measure the mass loss of various ingots as a function of temperature.
Figure 6 is a TGA plot of all the ingots made with compositions designated in Table 1. The data reveal that there is *no* significant weight loss by vaporization of selenium from ingots with compositions in regions I_1 (a, b, and c) and I_2. Significant weight loss is observed only from the selenium-rich regions designated I_3 and I_4. Therefore, ingots with compositions in regions I_1 and I_2 should show no selenium loss during deposition and will not require the use of chalcogenide-rich atmospheres.

Table 2: XEDS data of $CuInSe_2$ films fabricated by liquid-phase deposition.

Sample ID #	Film Composition (at%)
SBD 1	21.6 : 25.9 : 52.5
SBD 2	22.7 : 36.1 : 41.2
SBD 3	17.8 : 12.6 : 69.6
SBD 4	23.9 : 29.9 : 46.1
SBD 5	30.7 : 26.9 : 42.3
SBD 6	6.2 : 47.1 : 46.7
SBD 7	25.2 : 26.4 : 48.3
SBD 8	23.6 : 29.5 : 46.9
SBD 9	22.4 : 35.2 : 42.4

4.5 Layers Deposited by the Sliding-Boat Mechanism

The sliding-boat technique has proven to work very well for depositing $CuInSe_2$ films from the melt. For all films deposited so far, the chemical composition of the starting ingot material was $Cu_{33.3}In_{33.3}Se_{33.3}$. This composition lies in the largest primary phase field of the of the liquidus projection of the $CuInSe_2$ ternary equilibrium phase diagram in which α-$CuInSe_2$ is the first phase to precipitate from the growth solution. Table 2 lists the compositions of nine films we have obtained from this ingot composition. All films were analyzed by XEDS (X-ray energy-dispersive spectrometry) in a scanning electron microscope (Hitachi S-3000 SEM).

All films where deposited onto quartz substrates which where sputter coated with 1 μm of Mo followed by 100 nm of Cu. Therefore, since the same ingot was used for the deposited films, the only variable changed to produce films of varying composition was the thermal profile of the deposition itself. The ingots where either first undercooled to just below the liquidus projection and then slid over substrate or, alternatively, first slid over the substrate and then undercooled. For the deposition of III–V semiconductors, these two methods were shown to have different growth kinetics.

Different deposition times resulted in different thicknesses of the films. For example, film 2 was deposited for 15 min at 650 °C and had an average thickness of 2.7 μm, whereas film 5 was deposited for 2 h at 655 °C and had an average thickness of 44 μm. (In each case, the thickness was measured by a Sloan DekTakII profilometer.) Generally, higher deposition temperatures and longer deposition times resulted in films with smoother surface morphology.

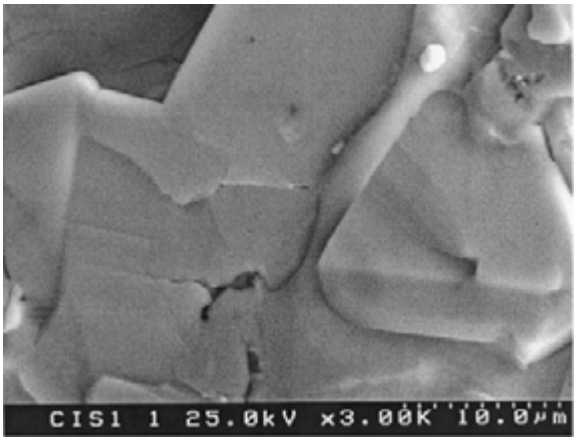

Figure 7: Surface morphology of an LPD-deposited film, exhibiting large grains with diameters > 10 μm.

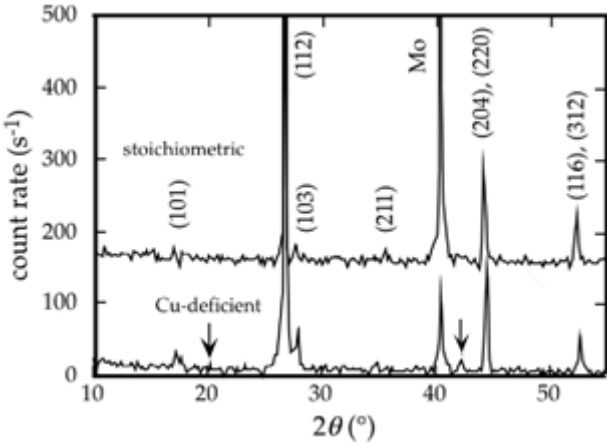

Figure 8: XRD pattern with strongest peak from the (112) growth plane (from sample SBD 3).

Figure 7 displays the surface morphology of sample SBD 2, revealing the presence of large grains with diameters > 10 µm. X-ray diffraction was also carried out to prove the existence of the chalcopyrite crystal structure as well as verify the presence of the preferred growth plane for CIS. The chalcopyrite crystal structure possessed by α-$CuInSe_2$ grows preferentially with facets parallel to {220}, {204}, or {112} planes. From Fig. 8 it is evident that the material has grown with the energetically preferred {112} surface.

Owing to the high viscosity of the Cu–In–Se melt, the thicknesses of the Cu–In –Se layers deposited in the beginning was relatively large – on the order of 10 to 15 µm. Apparently, the excessive thickness and roughness of the layers we deposited with the first-generation apparatus arose because the frozen material was able to lift the sliding boat.

To avoid this problem, we constructed a *second* sliding-boat apparatus. The major design change in this second construction are grooves that guide the sliding boat and keep it at constant height, such that the frozen material cannot lift it. Additionally, the new design offered better thermal contact between the melt and the thermocouple – different from the previous design, the tip of the thermocouple now resides directly beneath the substrate material.

Figure 9a shows a photograph of the reactor and the furnace. The re-designed sliding-boat is exposed in the enlargement of Fig. 9b. Again, the construction material we utilized was graphite because it is not wetted by the molten ingot material. Moreover, graphite possesses good thermal conductivity and is easily machinable. The red arrow in Fig. 9b points at the grooves guiding the sliding boat. As expected, the new construction enabled the deposition of thinner layers.

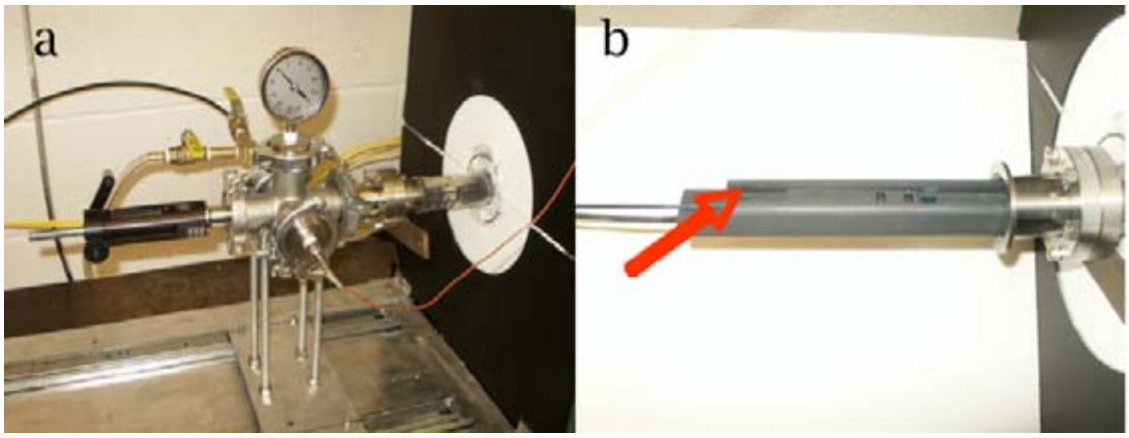

Figure 9: (a) The deposition reactor and the furnace. (b) Larger view of the new sliding-boat apparatus. The arrow points at groves guiding the boat to prevent the solidified material from pushing it up. This construction proved to be valuable for limiting the layer thickness.

Employing the new sliding-boat mechanism, we deposited several layers onto the quartz–1 μm Mo–100 nm Cu substrates. We confirmed that the stoichiometry of the newly deposited layers matched the desired stoichiometry of α-$CuInSe_2$. Moreover, XRD patterns revealed the dominant presence of grains with the chalcopyrite structure of α-$CuInSe_2$ with their surface parallel to {112} planes.

4.6 Single-Crystalline Substrates

In addition to improving the sliding boat mechanism, we have made several attempts to deposit α-$CuInSe_2$ onto (111) Si *single* crystals. The atomistic structure of the Si (111) surface has hexagonal symmetry and lattice parameters very close to those of the α-$CuInSe_2$ (112) surface; the lattice mismatch is only ≈6 %. Based on this similarity, one would expect that α-$CuInSe_2$ can grow *epitaxially* on (111) Si, i. e. as a single-crystalline layer with the same orientation as the substrate. Despite the similarity in structure, however, we have not succeeded so far in depositing α-$CuInSe_2$ onto Si substrates.

4.7 Grain Size

As demonstrated by the example of Fig. 7, the grain size of the layers we have obtained by liquid-phase deposition is large compared to any other deposition technique. To further analyze the grain size, we have employed conventional transmission electron microscopy (TEM), and in particular dark-field imaging (Section 4.11). This has revealed grains sizes in the range of 10 to 30 μm in diameter. The micrograph in Fig. 10 shows that even much larger, *macroscopic* grains can form by *dendritic* growth. Dendrites usually constitute regions with the same crystallographic orientation (although there may be small-angle grain boundaries within the dendrite). Dendritic growth can be explained by the details of heat transport through the melt and through the solid at the growth front. Since the area depicted in this micrograph is not an area that resided directly under the growth solution (ingot), but is from an area adjacent to it, the image provides valuable

insight into the wetting and crystallization behavior of α-$CuInSe_2$: dendritic growth usually indicates constitutional supercooling.

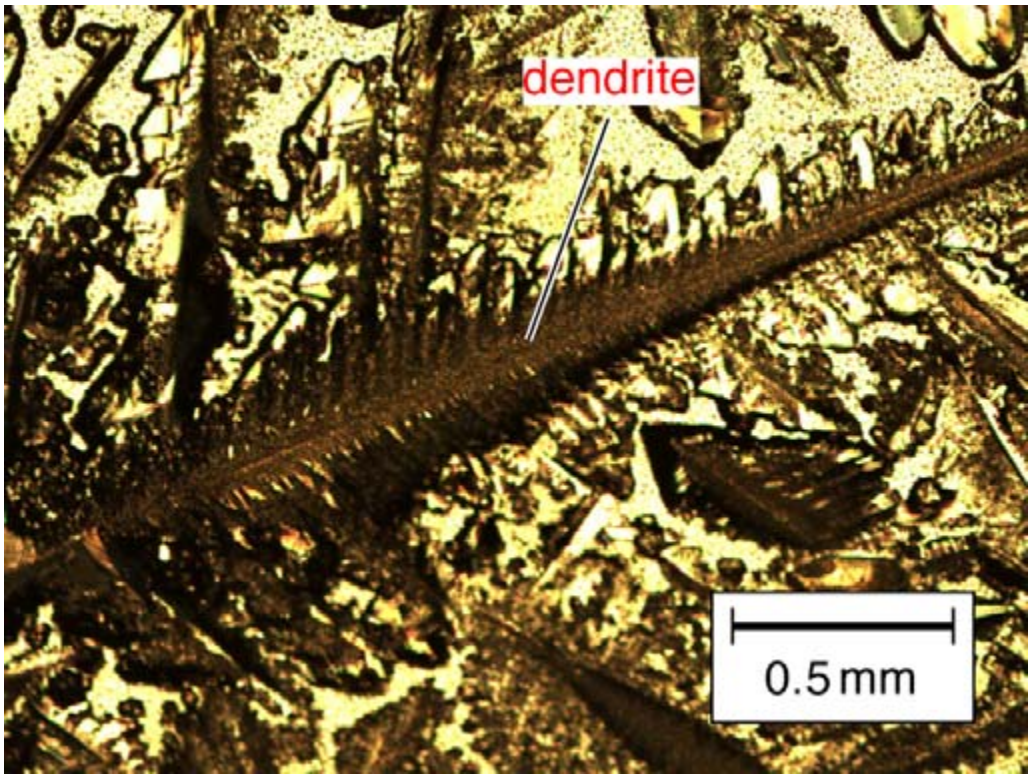

Figure 10: Optial micrograph of a layer made by liquid-phase deposition from the second-generation sliding-boat apparatus, revealing dentric growth of α-$CuInSe_2$.

4.8 Substrate Etching

To grow well-adherent, uniform films of a single phase, it is imperative to keep the substrate free of contaminants. Therefore, we set up the ability to etch substrates by two separate methods. First, an etch-back can be achieved with the use of the sliding boat since it contains two separate reservoirs. Loading one reservoir with the *substrate* material, contact with the substrate causes atoms at the substrate surface to dissolve into the reservoir, thus exposing a contaminant-free surface. An obstacle to this approach is that it requires choosing a substrate that possesses a proper work function to form an ohmic contact with α-$CuInSe_2$, and, at the same time, enables sufficiently high surface diffusivity at the deposition temperature.

Our second approach involved the use of a gas mixture containing an inert gas and hydrogen. After evacuating the deposition chamber and backfilling with argon several times, almost all of the oxygen was removed from the gas phase of the chamber. However, oxide scales remained on the surface of the substrate material. The purpose of

the hydrogen in the inert gas was to reduce the oxides, forming water vapor, which could then be removed by the pumps attached to the growth reactor.

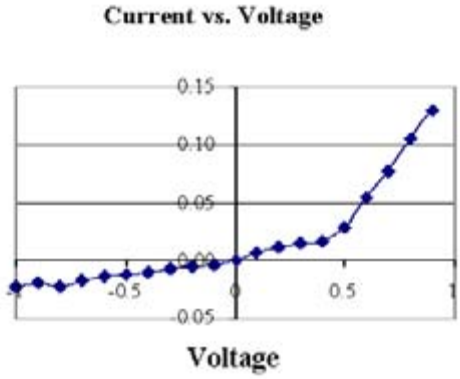

Figure 11: Current–voltage curve of an LPD-grown film, revealing rectifying behavior

4.9 Electrical Behavior

Sample SBD 4 proved to be one of the best samples grown thus far, with fairly uniform thickness of 55 μm and a bulk composition very close to α-$CuInSe_2$. Therefore, we used this material for electrical testing by preparing a Shockley diode from it. The diode was made by evaporating aluminum contacts directly to the surface if the CIS film. Figure 11 is a graph displaying a current–voltage curve of the first diode made from this project.

In addition to improving the methodology of liquid-phase deposition, we made attempts to fabricate a working solar cell. For this purpose, CdS layers were deposited onto the liquid-phase-deposited CIS layers by chemical bath deposition. Subsequently, we deposited ZnO layers by radio-frequency sputtering. Thus far, unfortunately, the resulting devices have failed. Apparently, the problem is that the volume of the deposited layers is so large compared to the melt reservoir that secondary, metallic phases form in the upper layers of the deposit. If this hypothesis is correct, it should be possible to eliminate the problem by implementing larger reservoirs for the liquid phase. This will minimize the compositional change of the melt during the deposition process and ensure that the composition remains inside the phase field in which α-$CuInSe_2$ is the primary solidifying phase.

4.10 Differential Thermal Analysis

For adjusting a sufficiently small supercooling during LPD of α-$CuInSe_2$ layers, as it is required for fabricating material with a low concentration of structural defects, it is important to know the precise liquidus temperature for the respective composition of the ingot. While the liquidus projection in (Fig. 1) indicates the liquidus temperature for every relevant composition, experimental verification is important to interpolate between

the isothermes and to accommodate deviations between the nominal and the actual composition.

A suitable method for determining the liquidus temperature is DTA (differential thermal analysis). Although a DTA apparatus was available at Case Western Reserve University, it was not suitable for the relatively high liquidus temperatures of up to 1073 K we needed to include in order to explore all four composition fields of Fig. 1. Moreover, we had special constraints concerning the specimen morphology arising from the need to keep the material encapsulated in a fused-silica tube. A suitable apparatus was eventually located at the NASA Glenn Research Center in Cleveland in the laboratory of Dr. A. Sayir, who kindly made this instument available to us.

Utilizing the DTA apparatus at the NASA Glenn Research Center, we determined the liquidus temperature of a suite of ingots by measuring the onset and outset temperatures of the first-order phase transformation of melting on the DTA plot; the liquidus temperature corresponds to the outset temperature during heating.

As an example, Fig. 12 shows the DTA plot for the ingot I1b of Table 1. The experimental liquidus temperature of 667 °C agrees well with the liquidus projection of Fig. 1. The small discrepancy originates from the fact that the composition lies slightly off the 700 °C isotherme.

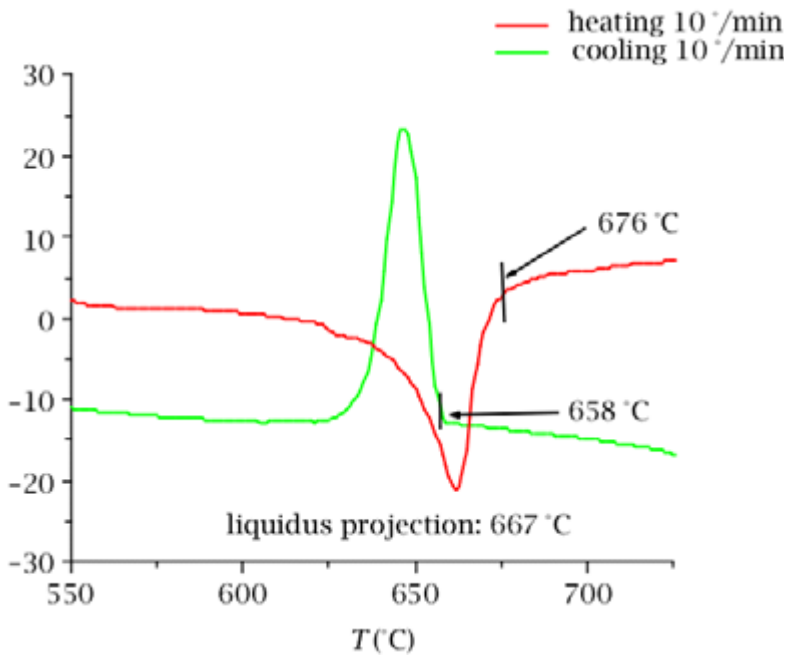

Figure 12: DTA (differential thermal analysis) of alloy I1b in Table 1.

While the information obtained by external DTA proved to be valuable, we found that trying to reproduce the measured liquidus temperature in our apparatus often resulted in multiphase films instead of the desired single-phase α-$CuInSe_2$ material. Apparently, there were discrepancies between the nominal and the actual temperature of the melt in our system.

To circumnavigate these issues, we added the capability to conduct *in situ* DTA in the sliding boat reactor. For this purpose, we had to modify the sliding boat somewhat. Another, more significant modification required to realize *in situ* DTA was that the ingot had to remain stationary, forcing us to alter the construction such that from then on the required movement between the melt and the substrate was realized by making the substrate slide back and forth underneath the deposition solution.
In the modified version of the system, two thermocouples – fed through the reactor – were located in the sliding boat mechanism. One of these was in contact with the ingot, while the other one served as a reference. Figure 13 displays the modified sliding boat mechanism with two thermocouples and the linkage for the linear motion manipulation of the underlying substrates.

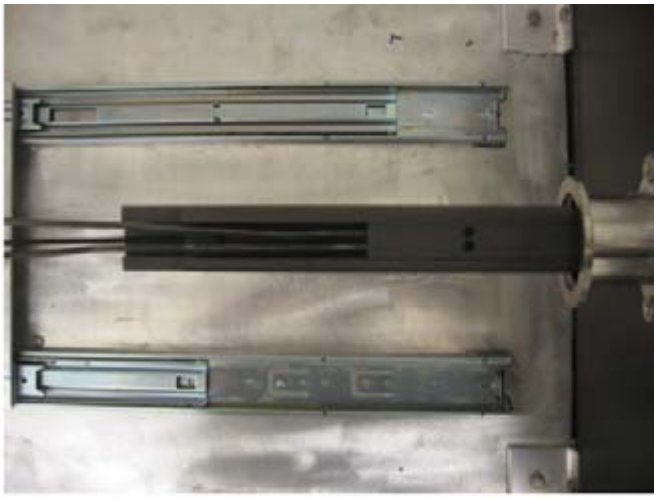

Figure 13: Modified sliding boat mechanism with two thermocouples and the linkage for the linear motion manipulation of the underlying substrates.

Figure 14: The entire system (LPD reactor and DTA) in its final version at the end of the project.

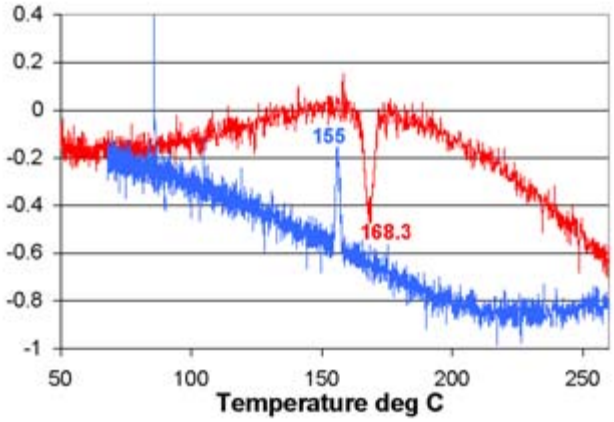

Figure 15: DTA of pure indium

The DTA was run by Labview software from a Windows XP platform. The data acquisition is achieved by a NI USB 9211 4 channel, 24 bit data acquisition card. The entire system (LPD reactor and DTA) can be seen in Figure 14. All reactor modifications and Labview programming where down in house. To test the new capability to perform *in situ* DTA analysis, pure indium was analyzed. Figure 15 shows the results from an initial measurement of indium. Upon heating, the acquired endothermal peak is found over ten degrees higher than the actual melting point of pure indium (T_m = 156.6 °C) due to the relatively high heating rate. Upon cooling, however, the corresponding exothermal peak is in excellent agreement with T_m, and this peak is the more relevant one for liquid-phase deposition of α-$CuInSe_2$. Initial attempts to use the *in situ* DTA for the deposition of α-$CuInSe_2$, however, failed because the thermocouple material underwent a chemical reaction with the growth solution. Presently, measures are being taken to circumvent this problem and provide the capability of *in situ* DTA for the deposition of α-$CuInSe_2$.

4.11 Transmission Electron Microscopy

4.11.1 Grain Size

TEM (transmission electron microscopy) confirmed that LPD is capable of producing CIS layers with very large grains, i. e. a very low density of grain boundaries.

Figure 16 presents bright-field and dark-field TEM images of deposited films containing α-$CuInSe_2$. In both images, regions of constant crystal orientations show up with the same gray level (dark in the bright-field image and bright in the dark-field image). Clearly, the film contains grains with a diameter exceeding several micrometers. Demonstrating this capability of liquid-phase deposition to provide films with a very large grain size constituted an important mile stone of our project. SAED (selected-area electron diffraction) patterns where obtained from the grain in Fig. 16 in , , and directions. The patterns display only one set of spots, confirming the existence of only one grain within the region of interest, and match simulated SAED patterns we have

obtained with the help of the JAVA Electron Microscopy Simulation software package "JEMS" (P. Stadelmann, EPFL, Lausanne) to within only 1 % deviation, both azimuthally and radially.

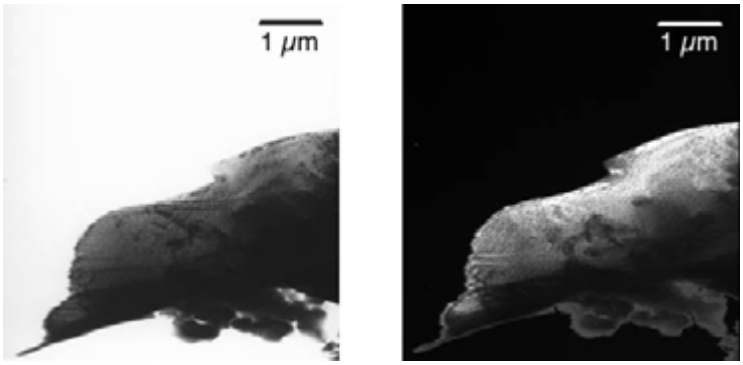

Figure 16: Bright field image on left (dark field on right) revealing course grain of deposited α-$CuInSe_2$.

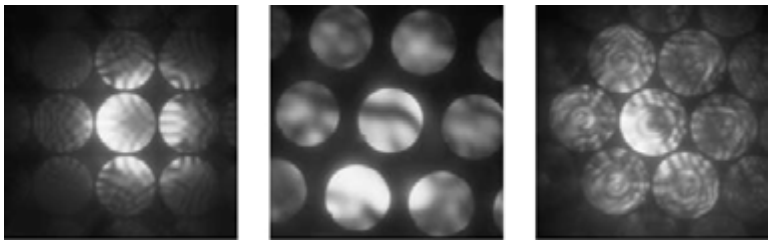

Figure 17: CBED patterns recorded in <110>, <110>, and <112> direction.

We need to point out, however, that these diffraction patterns alone are not sufficient to conclusively *prove* the existence of α-$CuInSe_2$. This is due to the fact that many phases of $CuInSe_2$, and in particular those that were identified in the compositional neighborhood of α-$CuInSe_2$, also possess tetragonal crystal lattices with lattice parameters very close to those of α-$CuInSe_2$. This circumstance makes it difficult to determine the phase of the deposited material by X-ray or conventional electron diffraction alone.
On the hand, simulated CBED (convergent beam electron diffraction) patterns of the phases in question should reveal distinct differences in the fine detail consisting of HOLZ (higher-order Laue zone) lines, thus enabling us to discern α-$CuInSe_2$ from undesired phases. Initial CBED patterns we obtained from the grain in Fig. 16 are shown in Fig. 17. However, these patterns merely exhibit Bragg fringes, not the required HOLZ lines. Accordingly, the quality of the TEM specimen as well as the CBED technique need further improvement.

Since we could not observe HOLZ lines yet, we determined the composition of the films from which the TEM specimen of Figs. 16 and 17 were prepared by XEDS (X-ray energy dispersive spectroscopy) in a scanning electron microscope. These measurements

indicated a Cu:In:Se ratio of 24:30:46. Along with the SAED patterns, this is strong evidence – although not a proof – for the existence of α-$CuInSe_2$.

5 Team Activities

The group at CWRU has actively participated in the National CIS Team Meetings with presentations about the project reported here and for a workshop on microcharacterization of $CuInSe_2$ thin films.

6 Conclusion

The work we were able to carry out constitutes a best effort under the financial and temporal constraints of this project. Partly because of these constraints and partly because of unforeseen obstacles, not all goals formulated in our proposal could be realized. However, we believe that our results demonstrate that liquid-phase deposition can be developed into a viable method for fabricating single-phase CIS (alpha-Cu–In–Se) films with a low density of structural defects and a correspondingly high performance in photovoltaic applications.

The results of our work demonstrate that the proposed technique is indeed capable of producing films with a particularly large grain size and a correspondingly low density of grain boundaries. In order to obtain films sufficiently thin for solar cell applications and with a sufficiently smooth surface, it is advantageous to employ a sliding boat mechanism.

Potential problems, as determined by our work, may arise from insufficient substrate wetting, melt viscosity, and insufficiently accurate determination of the liquidus (onset of solidification) temperature. In the course of the project, we have learned to deal with all three issues.

Future work on liquid-phase deposition of CIS should focus on the interaction between the melt and the substrate surface, the resulting CIS interfaces, the surface morphology of the LPD-grown films, and of course the electronic properties of the material.

From our interaction with members of the thin-film photovoltaics team (organized by NREL) and inter actions we had with potential industrial partners, we conclude that further developing this new method is scientifically and technologically rewarding.

Acknowledgment

We gratefully acknowledge the financial support we received from the National Renewable Energy Laboratory. We would also like to thank the project monitors, particularly Dr. B. von Roedern, for their continued interest in this project, and Dr. A. Sayir and Ms. A. Palcer for DTA measurements.

References

[1] T. Gödecke, T. Haalboom, and F. Ernst. Phase equilibria of Cu-In-Se. I. Stable states and non-equilibrium states of the In_2Se_3–Cu_2Se subsystem. *Zeitschrift für Metallkunde*, 91:622–634, 2000.

[2] T. Gödecke, T. Haalboom, and F. Ernst. Phase equilibria of Cu-In-Se. II. The Cu–Cu_2Se–In_2Se_3–In subsystem. *Zeitschrift für Metallkunde*, 91:635–650, 2000.

[3] T. Gödecke, T. Haalboom, and F. Ernst. Phase equilibria of Cu-In-Se. III. The In_2Se_3–Se–Cu_2Se subsystem. *Zeitschrift für Metallkunde*, 91:651–662, 2000.

[4] J. Cowen, L. Lucas, F. Ernst, P. Pirouz, A. Hepp, and S. Bailey. Liquid-phase deposition of single-phase alpha-copper-indium-diselenide. *Materials Science and Engineering B*, 116: 311–319, 2005.

[5] C. Persson and A. Zunger. Anomalous grain boundary physics in polycrystalline $CuInSe_2$: The existence of a hole barrier. *Physical Review Letters*, 91(26):266401–266404, 2003.

[6] F. Ernst, 2004. URL: http://dmseg5.case.edu/groups/Ernst/csam.html.

REPORT DOCUMENTATION PAGE

Form Approved
OMB No. 0704-0188

PLEASE DO NOT RETURN YOUR FORM TO THE ABOVE ORGANIZATION.

1. REPORT DATE *(DD-MM-YYYY)*	2. REPORT TYPE	3. DATES COVERED *(From - To)*
February 2006	Subcontract Report	February 2003 – July 2005

4. TITLE AND SUBTITLE
Liquid-Phase Deposition of CIS Thin Layers: Final Report, February 2003 – July 2005

5a. CONTRACT NUMBER
DE-AC36-99-GO10337

5b. GRANT NUMBER

5c. PROGRAM ELEMENT NUMBER

6. AUTHOR(S)
F. Ernst and P. Pirouz

5d. PROJECT NUMBER
NREL/SR-520-39341

5e. TASK NUMBER
PVB65101

5f. WORK UNIT NUMBER

7. PERFORMING ORGANIZATION NAME(S) AND ADDRESS(ES)
Case Western University
Dept. of Materials Science and Engineering
Cleveland, OH 44106

8. PERFORMING ORGANIZATION REPORT NUMBER
XDJ-3-30630-33

9. SPONSORING/MONITORING AGENCY NAME(S) AND ADDRESS(ES)
National Renewable Energy Laboratory
1617 Cole Blvd.
Golden, CO 80401-3393

10. SPONSOR/MONITOR'S ACRONYM(S)
NREL

11. SPONSORING/MONITORING AGENCY REPORT NUMBER
NREL/SR-520-39341

12. DISTRIBUTION AVAILABILITY STATEMENT
National Technical Information Service
U.S. Department of Commerce
5285 Port Royal Road
Springfield, VA 22161

13. SUPPLEMENTARY NOTES
NREL Technical Monitor: Bolko von Roedern

14. ABSTRACT *(Maximum **200 Words**)*

The goal of this project was to fabricate single-phase CIS (α-Cu–In–Se, stoichiometric composition: $CuInSe_2$) thin films for photovoltaic applications from a *liquid* phase – a Cu–In–Se melt of appropriate composition. This approach of "liquid-phase deposition" (LPD) is based on the new phase diagram we have established for Cu–In–Se, the first complete equilibrium phase diagram of this system. The liquidus projection exhibits four composition fields in which the primary solid phase, i.e., the first solid material that forms on cooling down from an entirely liquid state, is α-$CuInSe_2$. Remarkably, none of the four composition fields is anywhere near the stoichiometric composition ($CuInSe_2$) of α-$CuInSe_2$. The results demonstrate that the proposed technique is indeed capable of producing films with a particularly large grain size and a correspondingly low density of grain boundaries. To obtain films sufficiently thin for solar cell applications and with a sufficiently smooth surface, it is advantageous to employ a sliding boat mechanism. Future work on liquid-phase deposition of CIS should focus on the interaction between the melt and the substrate surface, the resulting CIS interfaces, the surface morphology of the LPD-grown films, and, of course, the electronic properties of the material.

15. SUBJECT TERMS
PV; liquid-phase deposition; thin film; electronic properties; grain size; copper indium diselenide (CIS); grain boundary; sliding-boat reactor;

`+			17. LIMITATION OF ABSTRACT	18. NUMBER OF PAGES	19a. NAME OF RESPONSIBLE PERSON
a. REPORT	b. ABSTRACT	c. THIS PAGE			19b. TELEPONE NUMBER (*Include area code)*
Unclassified	Unclassified	Unclassified	UL		

Standard Form 298 (Rev. 8/98)
Prescribed by ANSI Std. Z39.18